Theory of plasmon-enhanced high-order harmonic generation in the vicinity of metal nanostructures in noble gases

A. Husakou,* S.-J. Im, and J. Herrmann
Max Born Institute of Nonlinear Optics and Short Pulse Spectroscopy, Max Born Strasse 2a, D-12489 Berlin, Germany
(Received 2 July 2010; published 29 April 2011)

We present a semiclassical model for plasmon-enhanced high-order harmonic generation (HHG) in the vicinity of metal nanostructures. We show that, besides the field enhancement, both the inhomogeneity of the enhanced local fields and electron absorption by the metal surface play an important role in the HHG process and lead to the generation of even harmonics and a significantly increased cutoff. For the examples of silver-coated nanocones and bowtie antennas, we predict that the required intensity reduces by up to three orders of magnitude due to plasmonic field enhancement. The study of the enhanced high-order harmonic generation is connected with a finite-element simulation of the electric field enhancement due to the excitation of the plasmonic modes.

DOI: 10.1103/PhysRevA.83.043839 PACS number(s): 42.65.Ky, 78.67.Bf

Progress of contemporary ultrafast laser physics has led to the generation of attosecond laser pulses by high-order harmonic generation (HHG) [1], opening the way to exciting opportunities to study attosecond-resolved fundamental electronic processes in atoms and molecules [2–5]. On the other hand, in an another rapidly evolving field, metallic nanostructures were shown to realize localization of light on a subwavelength nanometer scale and huge plasmonic field enhancements in the vicinity of these objects [6,7]. Plasmonics has been the subject of extensive theoretical and experimental research [8]. Recently, an interesting experiment has been reported based on a combination of both fields: HHG has been demonstrated by nanojoule pulses directly from a laser oscillator by exploiting the local field enhancement near a metallic bowtie-shaped gold nanoelement [9]. The elimination of complex and expensive amplifiers and the opportunity to perform HHG and attosecond experiments at megahertz repetition rates can significantly extend the ability of extreme vacuum ultraviolet generation and attosecond pump-probe spectroscopy. However, a theoretical description of plasmon-enhanced HHG, which is crucial for further progress in this field, is currently missing.

This paper is a theoretical investigation of plasmon-enhanced HHG in a noble gas in the vicinity of a silver nanocone and a silver bowtie structure. In the vicinity of the metal nanostructures, the incident laser intensity is enhanced by up to three orders of magnitude by the plasmons in so-called hot spots, and sensitively depends on the position. This strongly enhanced field ionizes the noble gas atoms and accelerates the resulting electrons, which recollide with the parent ion, transforming their kinetic energy into coherent high-order harmonic radiation. However, in the vicinity of the nanostructure, two additional effects come into play. In the hot spot, electrons experience the inhomogeneous electric field, and some of them hit the metal surface and never return to the parent ion. We show that both field inhomogeneity and the electron absorption at the metal surface lead to the emission of even harmonics as well as to more than a twofold increase of the cutoff frequency.

*gusakov@mbi-berlin.de

We describe HHG in the framework of an extended Lewenstein model and start with the description of the standard version of this semiclassical approach. In the first stage, the strong electric field $\mathbf{E}(t)$ ionizes an atom at the time moment t_s and creates a free electron in the continuum. The free electron is accelerated by the oscillating field and for a linearly polarized field is driven back to the parent ion after the field changes the direction. In the last stage, the recombination with the parent ion at the moment t_f leads to the emission of a high-energy photon. The high-order harmonic signal is determined by the field-induced time-dependent dipole moment $d(t) = e\langle 0|x|\Phi_c(t)\rangle + \text{c.c.}$ where $\langle 0|$ is the ground state of the atom and $|\Phi_c(t)\rangle$ is the wave function tracing the evolution in the continuum state. Neglecting the Coulomb potential, one can represent the time-dependent high-order harmonic dipole moment in direction of the field polarization x as [10]

$$d(t_f) = ie^2 \int_{-\infty}^{t_f} dt_s \int d^3p \langle 0|x|p - eA(t_f)\rangle e^{iS/\hbar} \times E(t_s)\langle p - eA(t_s)|x|0\rangle + \text{c.c.} \quad (1)$$

In this expression, the intergration is performed over all past ionization moments t_s and all canonical momenta $p = m_e v + eA$, which is a conserved quantity in the external field. Here $\langle p - eA(t_s)|x|0\rangle = d_x[p - eA(t_s)]$ is the dipole moment for a transition from the ground state to the continuum with a kinetic momentum $p - eA(t_s)$, and $A(t)$ is the vector potential with $\dot{A} \equiv dA(t)/dt = E(t)$. During the second stage, this momentum state evolves freely, influenced only by the laser field, and acquires a phase factor $\exp[-iS(t_f,t_s)/\hbar]$, where $S(t_f,t_s) = \int_{t_s}^{t_f}\{I_p + [p - eA(t)]^2/2m_e\}dt$ is the classical action of the electron moving in the laser field, I_p being the ionization potential. Finally, the electron recombines with the parent ion into the ground state with the amplitude $d_x^*[p - eA(t_f)]$. Equation (1) can be simplified to [10]

$$d(t_f) = i\frac{e}{2\omega_0^{5/2}m_e}\int_{-\infty}^{t_f}\left(\frac{\pi}{\epsilon + i\Delta t/2}\right)^{3/2} H(t_f,t_s) \times d_x[p_{st} - eA(t_s)]\exp\left(-i\frac{S(t_f,t_s)}{\hbar}\right) \times d_x^*[p_{st} - eA(t_f)]E(t_f)dt_s + \text{c.c.} \quad (2)$$

Here, the canonical momentum is given by $p_{st} = e\Delta B/\Delta t$ with $\dot{B}(t) = A(t)$, $\Delta t \equiv t_f - t_s$, ϵ is an arbitrary small regularization parameter, ω_0 is the central laser frequency, m_e is the electron mass, and the action is $S_0(t_f,t_s) = I_p\Delta t - 0.5e^2(\Delta B^2/\Delta t + \Delta C)/m_e$ where $\dot{C}(t) = A^2(t)$. For any function F, we define $\Delta F \equiv F(t_f) - F(t_s)$. For the ground state of a hydrogenlike atom, the dipole matrix element is $d_x(p) = i2^{7.25}(\hbar\omega_0 m_e^2 I_p)^{5/4}\pi^{-1}p/(p^2+\alpha)^3$, where $\alpha = 2m_e^{1/2}I_p^{1/2}$. In the unmodified Lewenstein model, we have $H(t_f,t_s) \equiv 1$.

We extend the semiclassical HHG model, accounting for the inhomogeneity of the field in the hot spot by adding the first-derivative term to the field $E(t,x) = E(t)(1 + x/d_{inh})$, and consider this derivative term as a perturbation, including only the first-order correction $x^{(1)}(t) = -e/(d_{inh}m_e)\int_{t_s}^{t} dt' \int_{t_s}^{t'} E(t'')x^{(0)}(t'')dt''$ to the zeroth-order electron trajectory $x^{(0)}(t)$. The second-order term is smaller than 25% of the first-order one. As a result, the expressions for the momentum p_{st} and $S(t_f,t_s)$ are modified as follows:

$$p_{st} = e\left[A(t_s) + \frac{\Delta B - A(t_s)\Delta t + \beta[0.5(\Delta B)^2 - \Delta D + C(t_s)\Delta t]}{\Delta t - \beta\{2\Delta G + \Delta t[B(t) + B(t_s)]\}}\right], \quad (3)$$

$$S(t_f,t_s) = S_0(t_f,t_s) + e^2\beta m_e^{-1}\{p(t_s)^2\{2\Delta G + [B(t_f) + B(t_s)]\Delta t\} + p(t_s)(-\Delta C\Delta t + 2\Delta D) + [C(t_f) + C(t_s)]\Delta B - 2\Delta F\}, \quad (4)$$

where $\dot{D}(t) = C(t)$, $\dot{F}(t) = C(t)E(t)$, $\dot{G}(t) = B(t)$, and $\beta = e/(m_e d_{inh})$. Another modification of the model is described by the function $H(t,t_s)$ under the integral in Eq. (2). This function is equal to 1 unless the electron during the motion hits the metal surface positioned at d_{sur}; otherwise, we assume that the electron is absorbed by the surface and set $H(t,t_s) = 0$.

We have used the finite-element Maxwell solver JCMWAVE to model the plasmonic field enhancement in the vicinity of the nanostructure, taking into account the phenomenological complex-valued dielectric function of silver. For short input pulses, we included the dispersion of silver and the wavelength dependence of the enhancement factor near the nanostructure. In this paper, we disregard depolarization effects and the influence by next-nearest nanostructure, since the typical distance to them is much larger than the hot spot.

Typical intensities in the hot spots in the range of 10^{14}–10^{15} TW/cm^2 above the metal surface could lead to damage. However, the boundary condition for the electric field normal to the surface causes an intensity reduction of $1/|\epsilon_{Ag}|^2 \sim 0.01$ to values below 5 TW/cm^2. Therefore, for the considered parameters, the damage threshold of metal or metal nanoparticles of about 0.1 J/cm^2 [11] is not reached, in agreement with the experimental observations in [9], where no significant damage of the bowtie nanostructures was observed. For moderate laser intensities lower than 10 GW/cm^2, even and odd harmonics up to the fifth order can be generated from the metal surface [12] but efficiency very rapidly decreases with the harmonic order. For higher intensities below the relativistic values, no increase of high-order harmonic efficiency was reported. On the other hand, plasma formation and the multiphoton photoeffect [13] at the surface do not perturb the HHG process considered here. They exhibit features clearly distinct from the high-order harmonic spectra observed in the experiment [9] and in our simulations: the plateau-and-cutoff shape typical for the three-step HHG in gases.

We note that according to the previous experimental observations the nonlinear change of the metal dielectric function does not exceed the value of 2. The existence of the plasmonic modes is therefore not endangered by the optical metal nonlinearity; furthermore, it will only slightly influence the enhancement, which mostly arises from the nonresonant "lightning-rod" effect.

To understand the effect of the inhomogeneity of the field and of the metal surface on the HHG process, in Fig. 1 we consider the HHG spectra for different parameters d_{inh} [Fig. 1(a)] and d_{sur} [Fig. 1(b)] for cw radiation with a typical intensity in the hot spot of 200 TW/cm^2. The inverse spatial symmetry, present in the homogeneous infinite gas,

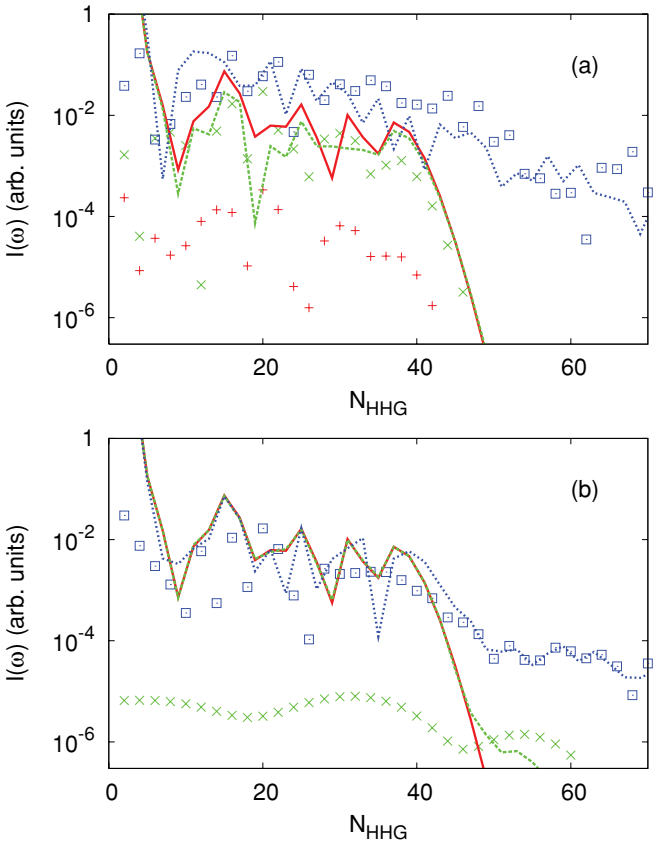

FIG. 1. (Color online) Influence of the field inhomogeneity (a) and of the metal surface (b) on the HHG process. Odd harmonics are presented by curves, while even harmonics are shown by points. In (a), the field has the inhomogeneity scales d_{inh} of 1000 nm (red solid curve and red vertical crosses), 20 nm (green short-dashed curve and green diagonal crosses), and 5 nm (blue long-dashed curve and blue squares). In (b), the distance to the metallic surface d_{sur} is 3 nm (red solid curve), 2.62 nm (green short-dashed curve and green diagonal crosses), and 1.5 nm (blue long-dashed curve and blue squares). For both cases, cw radiation at 830 nm with intensity in the hot spot of 200 TW/cm^2 in argon is considered.

is broken even for a very low inhomogeneity, characterized by $d_{\mathrm{inh}} = 1000$ nm, as shown in Fig. 1(a). This leads to a qualitatively new effect: the generation of even harmonics (shown by the blue crosses). For larger inhomogeneities with $d_{\mathrm{inh}} = 20$ nm, the amplitude of the even harmonics approaches that of odd harmonics. Simultaneously, the harmonic cutoff shifts to higher harmonic numbers and become much less pronounced. Due to inhomogeneity, electrons have higher velocities when they reach the parent ion, leading to a higher kinetic energy and therefore to a higher cutoff frequency. The influence of the metal surface and the associated electron absorption is studied in Fig. 1(b). One can see that for a distance to the surface $d_{\mathrm{sur}} = 3$ nm, no electron reaches the surface, and correspondingly no modification in the dipole moment and no even harmonics appear. For shorter d_{sur}, some electrons will reach the surface. Since the function $H(t,t_s)$ introduces a sharp modulation in the temporal profile of the harmonics, an extension of the spectrum to higher harmonic numbers can be seen in Fig. 1(b), combined with the emission of even harmonics. From Fig. 1, one can see that the combined effect of the field inhomogeneity and of the metal surface can increase the HHG cutoff by a factor larger than two.

Next, we perform a realistic simulation of HHG in the vicinity of a silver nanocone as depicted in Fig. 2(a). Such nanocone structure can be produced by silver deposition on a chemically created silicon needle without the need of nanoscale lithographic control. The curvature radius of the nanostructure edges is the key parameter determining the maximum field enhancement, with optimum structure having the smallest curvature radius. We have assumed a radius of 5 nm, in correspondence with the current state of the manufacturing technique. The spatial field distribution shown in Fig. 2(b) with parameters given in the caption demonstrates intensity enhancement factors of up to 1000 in the hot spot in the vicinity of the tip as well as only a weak azimuthal dependence. Note that the field is inhomogeneous on the scale below 10 nm in the hot spot, which is located directly above the metal surface. The parameters $d_{\mathrm{inh}}(x,y,z)$ and $d_{\mathrm{sur}}(x,y,z)$ are calculated from this spatial distribution of the field and are used for the HHG simulation by using the extended model as given by Eqs. (2)–(4). In Figs. 2(c) and 2(d), we present the spatial distribution of the harmonic cutoff N_{th} for an excitation by 830-nm sech-shaped pump pulses with intensity of only 0.3 TW/cm^2, full width at half-maximum (FWHM) of 10 fs, and polarization and wave vector as indicated in Fig. 2(a). The field enhancement in the hot spot increases the intensity to roughly 300 TW/cm^2, which for the chosen wavelength corresponds in the unmodified Lewenstein model to a cutoff roughly at the 50th harmonic, as can be seen in Fig. 2(c). However, due to the effect of the field inhomogeneity and the presence of the metal surface, the cutoff increases up to the 105th harmonic, which correspond to the emission of 150-eV photons. In Fig. 2(e), a comparison between the extended model including the effects of the field inhomogeneity and metal surface and the unmodified Lewenstein model is drawn. The cutoff harmonic number as a function of the position reaches values of 105 for the modified model, while the unmodified model predicts values of only 50. Further from the tip of the nanocone, the field become relatively homogeneous, and the distance to the metal surface is large; therefore, both models coincide. Note,

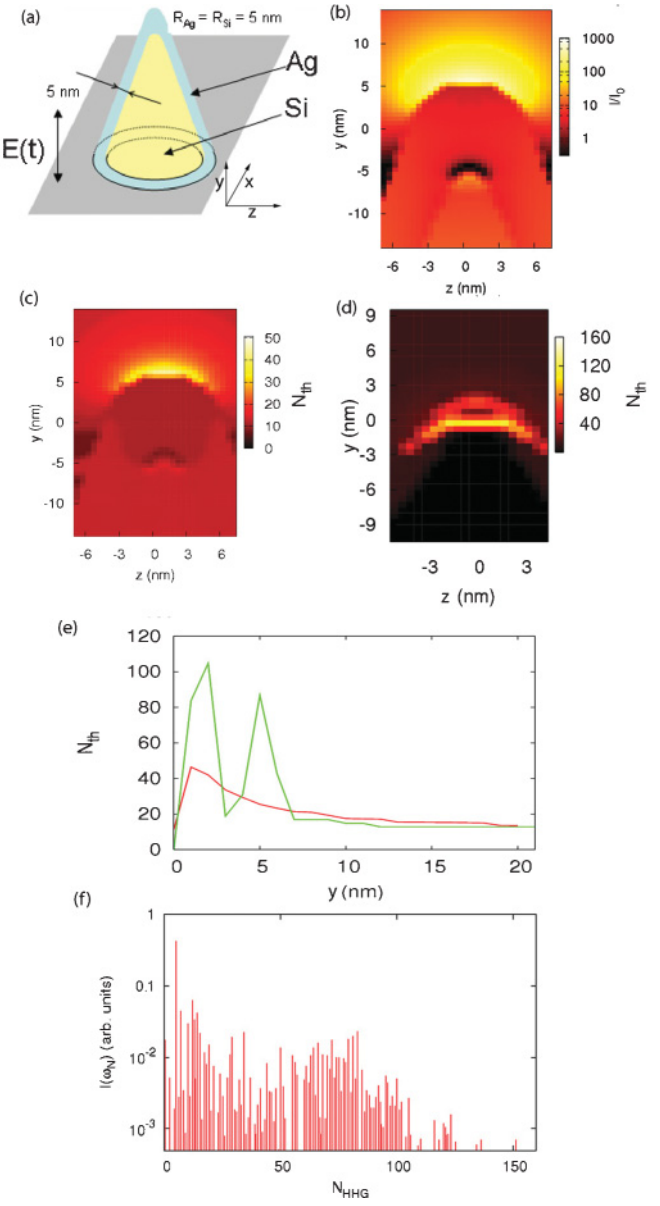

FIG. 2. (Color online) High-order harmonic generation in the vicinity of a nanocone structure. In (a), the scheme of the nanocone is shown. The curvature radii and the thickness of silver coating are 5 nm, and the y-polarized field propagates along the x direction. In (b), the intensity enhancement is presented for the zy cross section of the incident field at 830 nm. In (c) and (d), the distribution of the harmonic cutoff is shown for the model without (c) and with (d) modifications by the field inhomogeneity and metal surface for 10-fs input pulses with 0.3 TW/cm^2 intensity and argon surrounding the tip. In (e), the cutoff for the modified (green curve) and unmodified (red curve) model is shown along the y axis, and the spectrum for cw excitation with the above parameters is shown.

however, that although the modifications of the Lewenstein model are important only in a small fraction of the volume, it is exactly this volume (the hot spot) which dominates the generation of high harmonics, making these modifications especially important. This is clearly visible in Fig. 2(f), where we show the spectrum of the high harmonics emitted in the x direction integrated over the spatial position, with a

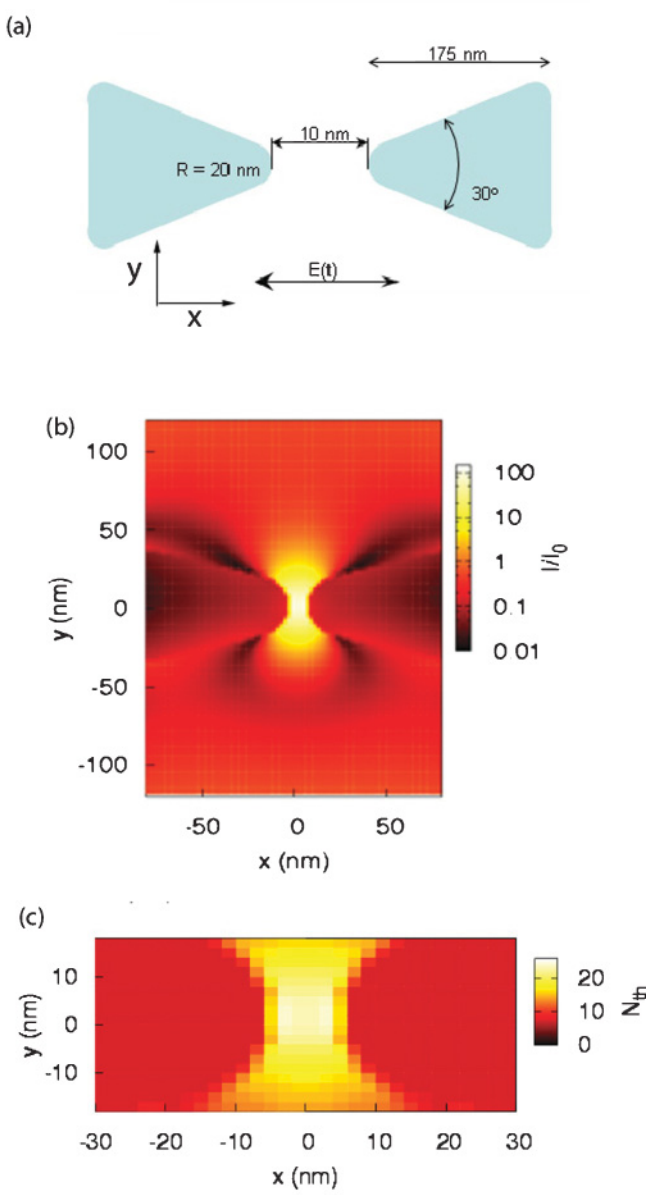

FIG. 3. (Color online) High-order harmonic generation in the vicinity of a bowtie structure. In (a), the scheme of the bowtie structure and its geometric parameters are shown; the x-polarized field propagates along y direction. In (b), the field enhancement is presented for the xy cross section of the incident field at 830 nm; in (c), the distribution of the harmonic cutoff is shown for 10-fs input pulses with 0.5 TW/cm^2 intensity for HHG in argon surrounding the bowtie structure.

significant emission of even harmonics as well as the extended and smoothed cutoff. We have also calculated the phases of the HHG harmonics separately for short and long electron trajectories and found that the modification of phases due to the field inhomogeneity is negligible for short trajectories but reaches $\pi/2$ for the long ones. However, this will not influence the divergence of the HHG radiation, since the hot spot is smaller than the typically considered wavelength and acts as a pointlike source. In the case of multiple nanoparticles distributed on a substrate, in the supplementary material [14] we calculated the variation of the high-order harmonic phases with different intensities depending on the transverse positions in the beam incident on the substrate. It is shown that in the considered example the phases change only slightly for different intensities within the beam for harmonic numbers below 50, which can be compensated by an appropriate curvature of the pump beam. For higher harmonic numbers, the phases show strong changes, resulting in beam distortion due to irregular spatial modulation.

In order to compare the results of our model with experimental measurements, we have simulated high-order harmonic generation in the vicinity of a bowtie nanoantenna, such as used in Ref. [9]. Structure and parameters of the studied bowtie antennas are shown in Fig. 3(a); the nanoannatennas consist of two silver isosceles triangles with curvature radius and a distance between the vertices in the range of 10 nm. In Fig. 3(b), the field enhancement by the bowtie antenna with parameters as given in the figure is presented, which shows a hot spot between the inner vortices of the triangles and a maximum enhancement of about 10^2. By using this field enhancement, HHG is calculated by using the extended model. In Fig. 3(c) for incident 10-fs pulses with intensity of 0.5 TW/cm^2, the spatial distribution of the threshold harmonic number N_{th} is presented. The calculated maximum harmonic number is 23, which corresponds to the wavelength of 36 nm. This is in good agreement with the experimental findings of [9], where harmonics down to 45 nm were observed. Note that both the parameters of the bowtie antenna and the input intensity are not exactly determined in [9], which can lead to deviations between theory and the experiment. In contrast to the nanocone, in the case of the bowtie antenna a relatively low field enhancement due to larger curvature radii leads to a smaller amplitude of electron motion, which, together with a relatively homogeneous field distribution, makes the model modifications less important than in the case of the considered nanocone. Our calculations predict that the cutoff value has increased by only roughly 20% due to the effects of the inhomogeneity and the metallic surface.

Additionally, we have studied the temporal profile of the generated harmonic pulse for the case discussed in Fig. 2 (see supplemetary material [14]). We predict the formation of a train of 150-as pulses after filtering out the harmonics with orders below 40. These attosecond pulses are shorter and less regular than the 200-as pulses calculated by the unmodifed model and a homogeneous field.

[1] M. Hentschel, R. Kienberger, C. Spielmann, G. A. Reider, N. Milosevic, T. Brabec, P. Corkum, U. Heinzmann, M. Drescher, and F. Krausz, Nature (London) **414**, 509 (2001).
[2] A. Paul *et al.*, Nature (London) **421**, 51 (2003).
[3] P. B. Corkum and F. Krausz, Nat. Phys. **3**, 381 (2007).
[4] F. Krausz and M. Ivanov, Rev. Mod. Phys. **81**, 163 (2009).
[5] G. Sansone *et al.*, Nature (London) **465**, 763 (2010).
[6] S. Nie and S. R. Emory, Science **275**, 1102 (1997).

[7] M. I. Stockman, in *Nonlinear Optical Materials* (Springer-Verlag, New York 1998).
[8] S. A. Maier, *Plasmonics: Fundamentals and Applications* (Springer, Berlin, 2007).
[9] S. Kim *et al.*, Nature (London) **453**, 757 (2008).
[10] M. Lewenstein, P. Balcou, M. Y. Ivanov, A. LHuillier, and P. B. Corkum, Phys. Rev. A **49**, 2117 (1994).
[11] K. Furusawa *et al.*, Appl. Phys. A **69**, S359 (1999).
[12] G. Farkas C. Toth, S. D. Moustaizis, N. A. Papadogiannis, and C. Fotakis, Phys. Rev. A **46**, R3605 (1992).
[13] F. Banfi C. Giannetti, G. Ferrini, G. Galimberti, S. Pagliara, D. Fausti, and F. Parmigiani, Phys. Rev. Lett. **94**, 037601 (2005).
[14] See supplemental material at [http://link.aps.org/supplemental/10.1103/PhysRevA.83.043839].